Journal of Solid State Chemistry 183 (2010) 2937–2944

Contents lists available at ScienceDirect

Journal of Solid State Chemistry

journal homepage: www.elsevier.com/locate/jssc

Structure distortion and magnetism in double perovskites $Ca_{2-x}La_xFeReO_6$ ($0 \le x \le 0.8$)

Minfeng Lü [a], Junjie Li [b], Heng Zou [c], Zhijian Wu [a], Jian Meng [a,*]

[a] State Key Laboratory of Rare Earth Resource Utilization, Changchun Institute of Applied Chemistry, Chinese Academy of Sciences, Changchun 130022, PR China
[b] Jilin Province Petrochemical Engineering Institute, Changchun 130021, PR China
[c] Jilin TV & Radio University, No. 6815 Renmin St., Changchun 130022, PR China

ARTICLE INFO

Article history:
Received 17 June 2010
Received in revised form
21 September 2010
Accepted 22 September 2010
Available online 29 September 2010

Keywords:
Double perovskites
Magnetic properties
Powder X-ray diffraction
Ab initio structural determination methods

ABSTRACT

The crystal structure and magnetism of $Ca_{2-x}La_xFeReO_6$ ($0 \le x \le 0.8$) double perovskites have been investigated. The samples with low doping ($x \le 0.4$) are found to crystallize with the monoclinic $P2_1/n$ superstructure, while those in the high doping ones ($x \ge 0.6$) have orthorhombic *Pbnm* superstructure. With the increase of an La doping, the anti-site defects increases, giving rise to highly disordered samples at the Fe and Re positions. At the low doping region ($x \le 0.4$), the compounds undergo a simultaneous structural and magnetic transition accompanying a slight increase of the Curie temperature. The increase of Curie temperature is discussed in terms of the structural change with doping.

1. Introduction

Double perovskites $A_2BB'O_6$ (A is the alkaline-earth or rare-earth ion, B and B' are transition metal ions) have been attracted intense interests in many applied and fundamental areas of solid state chemistry, physics, advanced materials and catalysis due to the diverse properties. The half-metallic A_2FeReO_6 [1,2] (A=Sr and Ca) and Sr_2FeMoO_6 [3] are particularly interesting because of their potential applications in magneto-electronic devices. Among them, Ca_2FeReO_6 was found to have both a noticeable Curie temperature (T_c) of 538 K [4] and an insulating feature [5]. When comparing Ca_2FeBO_6 (B=Re and Mo) with their Sr-based analogs, it was found that the reported T_c in the Re-based perovskites is much higher than that in the Mo-based perovskites [6], although the crystal parameters, e.g. the Fe–O–Mo (Re) angles, are roughly the same. This enhancement of T_c was thought of the existence of an additional pdd-δ ferromagnetic coupling in Ca_2FeReO_6 [7]. It has been proposed that carrier doping in double perovskites has been a very successful tool to reveal some of the most exciting new phenomena, i.e., a significant increase of T_c in the series $Sr_{2-x}La_xFeMoO_6$ [8]. An enhancement of T_c was attributed to an increase in the number of carriers in the spin polarized conduction band. Nevertheless, samples with high doping level exhibit a very high degree of anti-site disorder defects (ASDs), i.e., the presence of B atoms at B' positions and vice versa, which is known to promote antiferromagnetic correlations of the compound [9].

Carrier doping has been successful in the FeRe-based compounds, when an La is substituted onto the Sr site, but with a slight enhancement of ASDs [10]. The value of ASDs is found to be minimal for x=0 in $(La_{1+x}M_{1-x})CoRuO_6$ compounds (8% inversion for M=Sr and 0% for M=Ca) [11]. However, there are few reports about doping of lanthanide on Ca_2FeReO_6 as we have known. Since the difference in ionic radii of divalent alkaline-earth Ca^{2+}(1.34 Å) and trivalent La^{3+}(1.36 Å) cation is small (ionic radius taken from tables of Shannon for coordination number equal to 12, Ref. [12]). A cooperative tilts and rotations of the oxygen octahedral (ReO_6 and FeO_6 in our case) will be seen, as in Ca_2FeReO_6. Tilting of FeO_6 or ReO_6 octahedral induces the additional pdd-δ ferromagnetic coupling, which is associated with the enhancement of an enhanced T_c [7]. Consequently, T_c will probably be affected by the effective electron doping and structural distortion. Until the reliable information of structural and magnetic data are collected, it is difficult to obtain the information behind the physical properties in the series compounds concerning the degree of structural distortion and the possibility of the existence of an effective electron doping. With this aim, we have developed the present study of the crystal structure and magnetism for the double perovskites $Ca_{2-x}La_x$-$FeReO_6$ with nominal composition ranging 0–0.8.

In this paper, the crystal structural models of $Ca_{2-x}La_xFeReO_6$ ($0 \le x \le 0.8$) have been developed and checked by *Ab initio* structural determination methods. Hence, accurate structural studies allow us to extrapolate our conclusion that the gradual

* Corresponding author. Fax: +86 431 85698041.
E-mail address: jmeng@ciac.jl.cn (J. Meng).

0022-4596/$ - see front matter © 2010 Elsevier Inc. All rights reserved.
doi:10.1016/j.jssc.2010.09.032

enhancement of T_c was related to more distorted structure, due to the existence of additional pdd-δ ferromagnetic coupling as can be seen later.

2. Experimental

The samples were prepared by the solid state reaction. Stoichiometric amounts of CaO, La_2O_3, Fe_2O_3, ReO_3, and Re (different ReO_3/Re ratios for $Ca_{2-x}La_xFeReO_6$ are listed in Table 1) were mixed and pressed into pellets at 350 MPa. The pellets were then heated at 1200 °C during 12 h in an atmosphere of Ar (nominal purity 99.999%) with heating and cooling rates of 7 °C/min.

Powder X-ray diffraction (XRD) measurements were performed on a Bruker D8 Focus diffractometer with Cu $K\alpha$ radiation. For phase identification, a normal scan (4°/min) was performed. The refinement data were collected on the powder samples using a step scan mode with a step size of 0.02° and a counting time of one second per step in the range 2θ 10–120°. The powder diffraction pattern of $Ca_{2-x}La_xFeReO_6$ was indexed with DICVOL04 [13] TREOR [14], ITO [15] based on the first 20–26 peaks, which were determined by peak fitting program XFIT [16]. The unit-cell parameters and space groups were confirmed further by the program Checkcell [17].

After LeBail [18] refinement via the GSAS Program [19], the structure solution was attempted by a direct approach, using SHELX [20] and DIRDIF [21]. We also used the software OVERLAP [22] to eliminate separated reflection in less than a chosen angular distance (0.04° 2θ). The three-dimensional Fourier map has been calculated using the observed structural factors determined from Le Bail's extraction and phase angles determined by Ca, Fe, Re and O atoms with SHELX via Wingx [23].

Finally, Rietveld refinements were done using the program GSAS [19], including the impurity phases. Profile functions III was chosen in order to correct asymmetry of low angle peaks for low doping samples ($x \leq 0.4$). Constraint was used when calculating the occupancies of Fe and Re, where the occupancies of Fe and Re were varied, while the total occupancy of Fe and Re was kept to one unit. The movements of oxygen were also constrained, detailed descriptions were found elsewhere [24].

Magnetic measurements were carried out between 5 and 750 K by a commercial Quantum Design (SQUID) magnetometer and LakeShore VSM-735.

3. Results

The room temperature XRD patterns correspond to single phase $Ca_{2-x}La_xFeReO_6$, except for small of amounts of impurity phases, as listed in Table 1. These impurities phases were included in the refinements of the corresponding samples. In the previous studies, the undoped sample Ca_2FeReO_6 crystallizes in the $P2_1/n$ space group [2,25], corresponding to the $a^-a^-b^+$ tilt system [26] in the notation of Glazer [27]. The tilts give rise to small displacement of the oxygen atoms from the ideal cubic positions and new diffraction peaks come up, as seen in Fig. 1. All diffraction peaks for the low doping samples ($x \leq 0.4$) can be well described in the space group $P2_1/n$, which may be depended on tolerance factor (t) on the supposition that B, B'ions arrange in complete 1:1 ordered manner. If t is less than unity, the monoclinic cell will be favored. As mentioned earlier, there is a small difference in ionic radii of A-sites cation. Thus, for $x=0$, $x=0.2$, and $x=0.4$, the space group $P2_1/n$ can be assigned, which is usually adopted by 1:1 ordered B-site double perovskites [28].

For samples $x=0.6$ and 0.8, two space groups *Pbnm* (No. 62) and $P21/n$ (No.14) have been analyzed. Although the superstructure reflection peak, suggesting a small degree of ordering, can be observed in low angle region of X-ray patterns (Fig. 1), the reasonable fit of the X-ray patterns are achieved within the completely disordered model of the space group *Pbnm*, which corresponds to the same octahedral tilt system as in the $P2_1/n$ space group. The model of space group *Pbnm* gives better reliability factors than $P21/n$ space group in terms of the obtained inter-atomic distances and the fit between observed and calculated diffraction patterns in high angle region.

From Fig. 1, we also noted that the intensity in the superstructure reflection (0 1 1) decreases with the increase of an La doping, which is an indication of the increase of ASDs. Therefore, the structural transformation from space group $P2_1/n$ to space group *Pbnm* is companied by rearrangement of the B-sites ions from the order to disorder with the increase of an La doping. Figs. 2(a) and (b) show the observed, calculated, and difference curves after Rietveld refinement of the powder X-ray diffraction data at room temperature for $Ca_{1.8}La_{0.2}FeReO_6$ and $Ca_{1.2}La_{0.8}FeReO_6$. Structural parameters, atomic positions, and R factors obtained from the analysis are summarized in Table 2.

Fig. 3 shows the lattice parameters obtained from the refinement as a function of an La doping. An apparent cell expansion upon an La doping can be observed. The expansion of the unit cell volume upon an La doping with a relatively larger

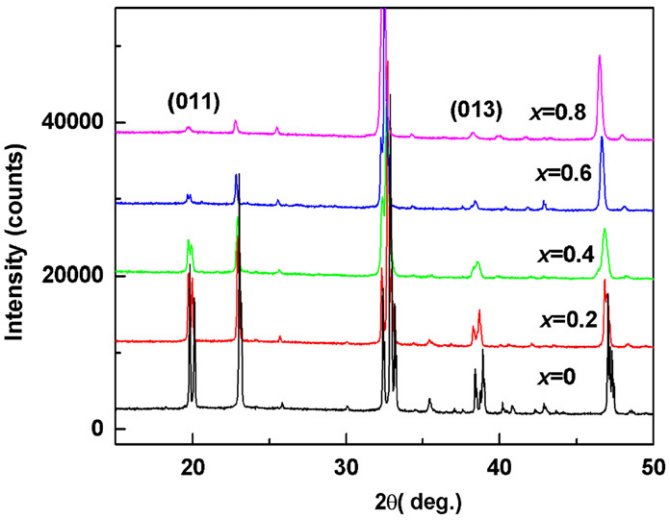

Fig. 1. X-ray diffraction patterns at room temperature of the $Ca_{2-x}La_xFeReO_6$ series.

Table 1
The experimental condition and the outcome of the impurities for $Ca_{2-x}La_xFeReO_6$.

	$x=0$	$x=0.2$	$x=0.4$	$x=0.6$	$x=0.8$
ReO3/Re ratio	5:1	4.77:1	5:1	4.33:1	3:1
Impurity, Fe_3O_4(atom%)	4.3	1.8	1.0	0	0
Impurity, Re (atom%)	3.1	0	1.0	3.8	0.6

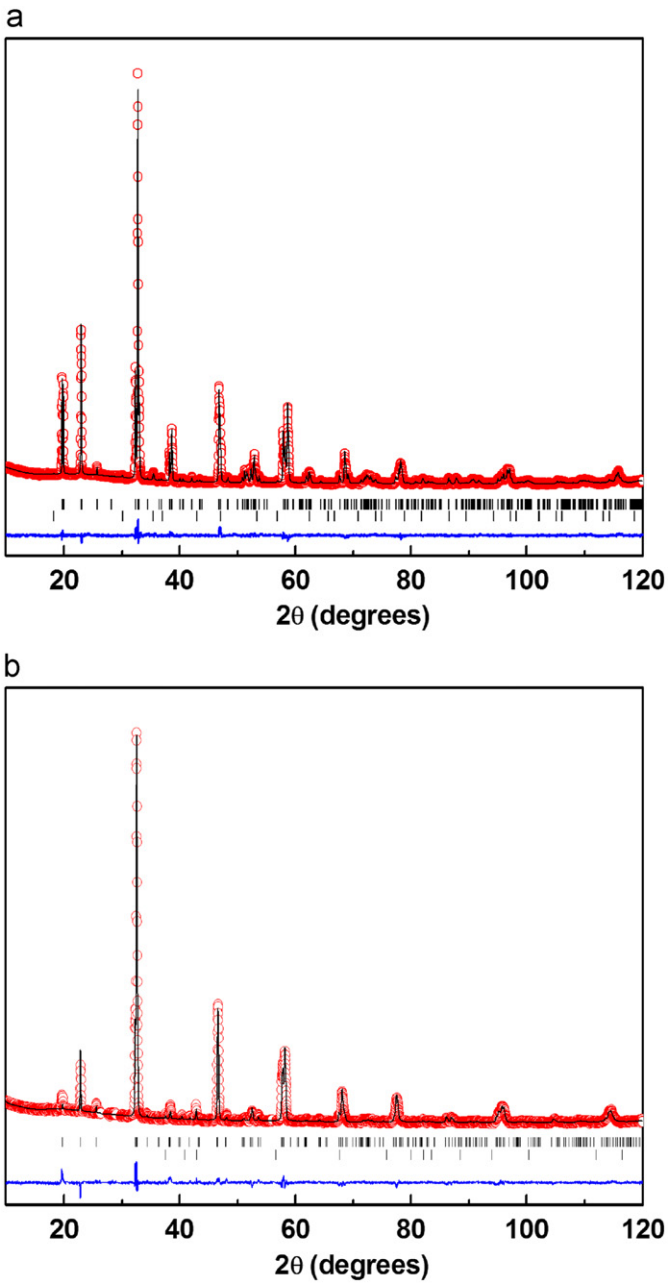

Fig. 2. Observed (red circles) and calculated (continuous black line) X-ray intensity profiles for $Ca_{1.8}La_{0.2}FeReO_6$ (a) and $Ca_{1.2}La_{0.8}FeReO_6$ (b). The short vertical lines indicate the angular position of the allowed Bragg reflections for the main phase (upper) and for the impurity phase (lower) (a) Fe_3O_4 and (b) Re. At the bottom in each figure the difference plot, I_{obs}–I_{calc}, is shown. (For interpretation of the references to color in this figure legend, the reader is referred to the web version of this article.)

volume cation is in accordance with what one expects according to Vegard's law. However, the cell expansion is probably motivated by the steric effects associated with the ionic sizes or electronic effects connected with carrier doping. On one hand, an expansion of the atomic species at B' sites in $(A_{2-x}A_x)BB'O_6$ was thought to be promoted by the electronic effects. On the other hand, the enhancement of the size of the A-sites leads to an increment of the Goldschmidt tolerance factor t, thus, the variance of actual mean radius, actual coordination number of A-sites ions, giving steric effects upon an La doping. It is worth noting that the expansion of the b-axis is small, compared with that of the a- or c-axis. Notice that the spontaneous magnetization axis for Ca_2FeReO_6 at room temperature was found to lie in the ac plane, 55° off a-axis [5]. Consequently, the expansion of the b-axis is associated with magnetoelastic coupling [29].

Fig. 4 shows the relevant structural parameters, the bond distances with the increase of an La doping (detailed parameters are shown in Table 3). In the low doping region ($x \leq 0.4$), the axial distances along the c-axis gradually increase with La doping for an ReO_6 octahedral, but dramatically an increase for FeO_6 octahedral. In the high doping region ($x \geq 0.6$), both Re–O and Fe–O bond distances nearly unchanged with the increase of La doping. In the ab plane (basal plane of the oxygen octahedral), the average bond distances of Re–O and Fe–O increase slightly in both low doping region ($x \leq 0.4$) and high doping region ($x \geq 0.6$). Since there is a significant amount of disorder in the high doping region ($x \geq 0.4$), those bond distances in Fig. 4 describe only the average structure, rather than a detailed local bonding. Concerning the bond angles, selected ones and their standard deviations have shown in Table 3.

Fig. 5(a) shows the magnetization curve measured at 5 K for $x=0.2$, $x=0.6$ and $x=0.8$. For the low doping samples ($x \leq 0.4$), the unusual shape of the low temperature hysteresis curves was observed, which could be explained by a superposition of two magnetic phases with different coercivity [25]. For high doping samples ($x \geq 0.6$), magnetization hysteresis loops go back to normal with a substantial increase in coercivity. Under the simplest ferrimagnetic arrangements, two couplings of ionic configurations Fe^{+3}–Re^{+5} and Fe^{+2}–Re^{+6} will lead to a saturation magnetization of 3 μ_B/f.u. (spin only ionic model). Deviation from this value in these compounds is normally explained as ASDs. As shown in Fig. 5(b) (right axis), the degree of ordering decreases with the increase of La concentration, x. It is worth noting that the degree of ordering, as expressed in Fig. 5(b), means the percentage atoms that are not misplaced in the rock-salt structure, 100% corresponding to a fully ordered sample, and 0% to a sample showing a random distribution of Fe and Re cations over B positions of the perovskites. We note that the La doping has caused the reduction of the saturation magnetization, due to the increasing disorder of the Fe/Re sublattices.

Fig. 6(a, b) showed magnetization hysteresis loops at a selected temperature for $x=0.4$ and 0.8 samples. Fig. 6(c) showed coercive field as a function of an La doping at a selected temperature. The coercivity increases with the increase of the doping level. This clearly indicates that the ferromagnetic behavior is quenched, while the AFM correlations contributed by ASDs increase. Moreover the ASDs and the saturation magnetization vary with x at the same trend. With the aim to investigate the change of magnetic properties, a detailed analysis of the transition of magnetism, structure and effects of ASDs are presented. Fig. 7(a) showed temperature dependence of magnetization. Teresa et al. proposed that the decrease of magnetization correlates with the simultaneous magnetic/structural transition occurring at T_S [29]. Therefore, the magnetic behaviors at temperature above and below T_S, in the selected samples, have been studied. The exact value of T_S was defined as the maximum of the derivative of the magnetization versus temperature (Fig. 7(b)). In Fig. 6(b), $x=0.8$ sample do not show any transition, with a slightly larger coercivity at 5 K than at 200 K,which can be regarded as a normal magnetic behavior. However, the behavior for $x=0.6$ at $T_S \approx 110$ K is quite different. First, the magnetization under 7 T decreases below 200 K. Second, the coercive field is substantially higher, more than 2 times larger at 5 K than at 200 K. Thus, we might determine the sample of $x=0.6$ as a transition point between a normal magnetic behavior ($x=0.8$) and abnormal ones ($x \leq 0.4$) after checking the thermal magnetization of each sample. When $x \leq 0.4$, many experimental results were very close. For an instance, T_S is 134 K for $x=0$ and the coercive field increases more than a factor

Table 2
Structural parameters for $Ca_{2-x}La_xFeReO_6$ at room temperature.

		$x=0$	$x=0.2$	$x=0.4$	$x=0.6$	$x=0.8$
a (Å)		5.4002(1)	5.4320(1)	5.4521(1)	5.4772(1)	5.5016(1)
b (Å)		5.5251(1)	5.5332(1)	5.5355(1)	5.5433(1)	5.5477(1)
c (Å)		7.6826(1)	7.7208(1)	7.7482(2)	7.7798(1)	7.8098(2)
β (*deg.*)		90.067(1)	90.063(2)	90.112(4)		
V (Å^3)		229.23	232.06	233.84	236.21	238.37
R_{wp} (%)		3.73	2.91	3.68	4.14	3.44
R_p (%)		2.60	2.24	2.74	2.88	2.58
R_F2 (%)		8.15	6.65	8.90	9.67	6.48
χ^2		3.47	1.84	2.81	3.17	2.49
Ca/La	At 4e(x y z)				At 4c(x y 1/4)	At 4c(x y 1/4)
	x	0.4950 (2)	0.4893 (6)	0.4737 (4)	0.0140(4)	−0.0120(4)
	y	−0.0470 (4)	−0.0393 (7)	−0.0309 (7)	−0.0283(5)	−0.0325(6)
	z	0.2509 (5)	0.2506 (10)	0.2499 (4)		
	Uiso(Å 2)	0.0222(2)	0.0045(5)	0.0054(6)	0.0114(6)	0.0109(7)
	Occupancy	1/0	0.9/0.1	0.8/0.2	0.7/0.3	0.6/0.4
Fe1	At 2d(0 0 0)				At 4b(1/2 0 0)	At 4b(1/2 0 0)
	Uiso(Å 2)	0.0177(3)	0.0243(7)	0.0219(5)	0.0142(3)	0.0208(4)
	Occupancy	0.983	0.919	0.842	0.5	0.5
Re1	At 2d(0 0 0)					At 4b(0 1/2 0)
	Uiso(Å 2)	0.0177(3)	0.0243(7)	0.0219(5)	0.0142(3)	0.0208(4)
	occupancy	0.017	0.081	0.158	0.5	0.5
Re2	At 2c(1/2 1/2 0)					
	Uiso(Å 2)	0.0167(4)	0.0119(3)	0.0155(6)		
	occupancy	0.983	0.919	0.842		
Fe2	At 2c(1/2 1/2 0)					
	Uiso(Å 2)	0.0167(4)	0.0119(3)	0.0155(6)		
	occupancy	0.017	0.081	0.158		
O1	At (x y z)				At 4c(x y 1/4)	At 4c(x y 1/4)
	x	0.1985 (3)	0.2099(7)	0.1937 (4)	0.0885(3)	0.0856(5)
	y	0.7118 (4)	0.7007(4)	0.6919 (6)	0.5192(6)	0.5163(4)
	z	1.0228 (5)	1.0328(5)	1.0183 (7)		
	Uiso(Å 2)	0.0114(4)	0.0105(8)	0.0119(2)	0.0084(6)	0.0077(7)
O2	At 4e(x y z)				At 8d (x y z)	At 8d (x y z)
	x	0.3005 (6)	0.2977 (5)	0.3060 (5)	0.7439(5)	0.7402(4)
	y	0.2219 (7)	0.2059 (4)	0.1999 (3)	0.2581(4)	0.2598(6)
	z	1.0546 (5)	1.0543(4)	1.0309 (4)	−0.0480(5)	−0.0520(5)
O3	Uiso(Å 2) At 4e(x y z)	0.0144(2)	0.0105(8)	0.0119(2)	0.0193(6)	0.0242(3)
	x	−0.0703 (3)	−0.0900 (11)	−0.1310 (3)		
	y	0.0109 (3)	0.0302 (5)	−0.0307 (6)		
	z	0.2538 (4)	0.2491 (4)	0.2567 (5)		
	Uiso(Å 2)	0.0144(4)	0.0105(8)	0.0119(2)		

of six larger at 5 K than at 200 K. The $x=0.2$ sample with $T_S \approx 105$ K, coercive field at 5 K is roughly 2 times larger than at 200 K, and more than a factor of 3 for $x=0.4$. However, its T_S should be in a range 40–120 K (average value is 80 K). In addition, two issues should be stressed: (i) there is a decrease of T_S as a function of an La doping and (ii) although the sample exhibits the abnormal magnetic loops, a saturation magnetization increases when the temperature drops below 200 K.

Fig. 8 shows the evolution of magnetization versus temperature. Curie temperature was calculated from the first derivative of an $M(T)$ curve. The value of T_c first increases at low doping level, reaches maximum 560 K at $x=0.4$, which is higher than that of the undoped compound Ca_2FeReO_6 (538 K), then drops. Clearly, two different regions were divided based on the variation of T_c and the magnetic response. At low doping level ($x \le 0.4$), the compounds are ferromagnets, and Curie temperature tends to increase with the increase of an La doping. The subtle increase of T_c in $Ca_{2-x}La_xFeReO_6$ series ($x \le 0.4$) can be qualitatively explained by structural and band hybridization effects. In magnetic oxides with perovskites structure, T_c has been claimed to be controlled by an electronic bandwidth [7,30]. For $x \ge 0.6$, Curie temperature decreases with x. The ferromagnetism becomes marginal, while antiferromagnetism promoted by ASDs becomes dominant, which introduce magnetic frustration into the system.

For perovskites ABX_3 compounds, the bandwidth W depends on both the B–X–B bond angles and B–X bond lengths, through the overlap integrals between the 3d orbitals of the metal ion B and the 2p orbitals of the anion X in the tight-binding approximation. The following formula has been applied to describe this double dependence

$$T_c \propto W \propto \cos\omega / d_{B-X}^{3.5}$$

where ω (given by $[\pi-(\text{B–X–B})]/2$) is the "tilting" angle in the plane of the bond and d_{B-X} is the bond length between B and X. For $x \le 0.4$, the deviation of the bond angle from 180° leads to a decrease of $\cos\omega$ as La doping increases. Increase of $d_{Fe/Re-O}$ together with the decrease of $\cos\omega$ will decrease the electronic bandwidth and, consequently, decrease of T_c. This conclusion is in disagreement with the experimental finding. However, an additional mechanism [7] has explained the anomalous increase of T_c for the compounds Ca_2FeReO_6. Deviations of the Fe–O–Re angle from 180° not only bring about a finite density of states of Fe/Re (e_g)

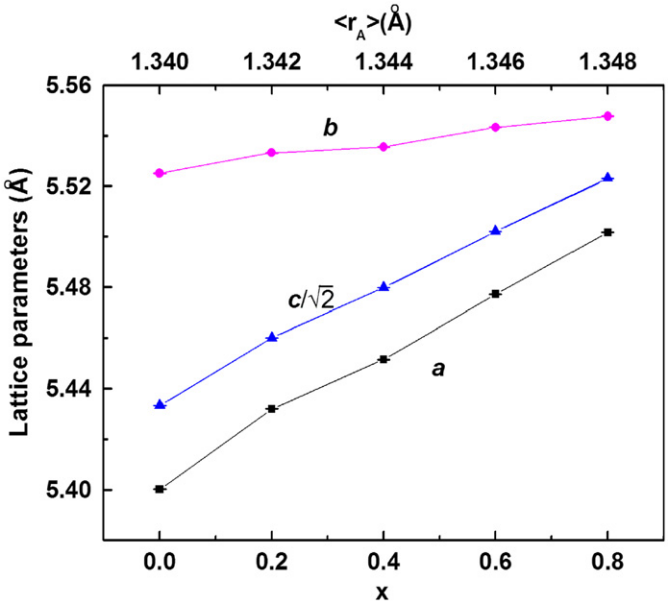

Fig. 3. Lattice parameters obtained from the refinement as a function of La content (x) (bottom axis) and average cationic size at A-sites (top axis).

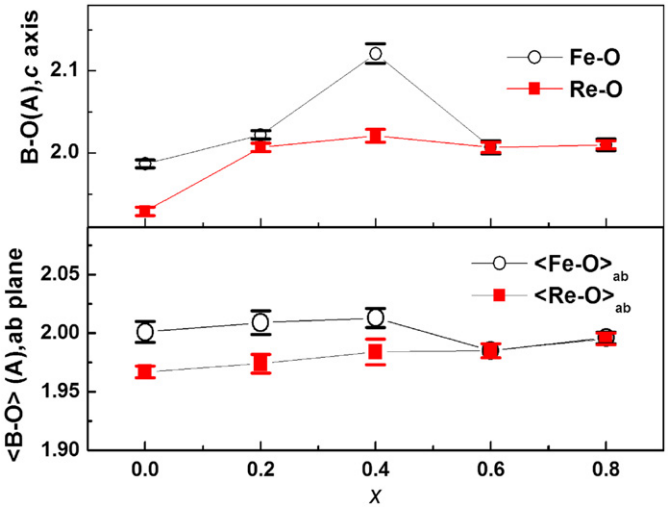

Fig. 4. Evolution of the bond distances B–O with La doping; (a) along the c-axis, and (b) in the basal plane of the oxygen octahedral (ab).

orbitals at the Fermi level, but also promote a nonzero Fe(e_g)–Re(e_g) pdd-δ ferromagnetic coupling. Therefore, this additional ferromagnetic coupling can also explain abnormal experimental results of $x \leq 0.4$.

4. Discussion and conclusion

By analyzing the experimental results, connections between structure and magnetic properties of the $Ca_{2-x}La_xFeReO_6$ series can be established. As can be inferred from Fig. 5(b), reducing of the saturation magnetization attributed to the promotion of antisite defects when the La content increases. However, large deviation from the linear behavior is noticed for $x \geq 0.6$. Therefore, two distinct regions can be defined. The low-doped samples ($x \leq 0.4$) exhibit monoclinic symmetry, ferromagnetic behavior,

Table 3
Selected bond lengths (Å) and angles (°) for $Ca_{2-x}La_xFeReO_6$.

	$x=0$	$x=0.2$	$x=0.4$	$x=0.6$	$x=0.8$
Re–O1 × 2	2.012 (3)	1.944 (8)	1.984 (5)	2.007(5)	2.010(4)
Re–O2 × 2	1.922 (5)	2.004 (7)	1.983 (11)	1.993(6)	1.997(5)
Re–O3 × 2	1.929 (5)	2.007 (5)	2.021 (8)	1.976(8)	1.995(7)
Fe–O1 × 2	1.927 (4)	2.026 (10)	2.010 (8)	2.007(5)	2.010(4)
Fe–O2 × 2	2.076 (9)	1.992 (6)	2.016 (7)	1.993(6)	1.997(5)
Fe–O3 × 2	1.987 (5)	2.022 (5)	2.121 (12)	1.976(8)	1.995(7)
⟨Fe–O⟩c	1.987	2.022	2.121	2.007	2.010
⟨Fe–O⟩ab	2.001	2.009	2.013	1.985	1.996
⟨Fe–O⟩	1.997	2.013	2.049	1.992	2.000
⟨Re–O⟩c	1.929	2.007	2.021	2.007	2.010
⟨Re–O⟩ab	1.967	1.974	1.984	1.985	1.995
⟨Re–O⟩	1.954	1.985	1.996	1.992	2.000
Re–O1–Fe	157.2 (3)	155.0(5)	153.0(4)	151.3(5)	152.4(4)
Re–O2–Fe	149.9 (5)	148.3(2)	152.4(4)	158.0(4)	156.1(6)
Re–O3–Fe	157.3 (4)	150.0(3)	138.4(7)		
⟨Re–O–Fe⟩[a]	154.8(5)	151.1(5)	147.9		
ω	12.6	14.5	16.0		

[a] For the $P2_1/n$ symmetry, there different values of Re–O–Fe angles, in the paper we refer to its average.

and abnormal coercivity at 5 K, and a tendency to increase T_c. The high-doped samples ($x \geq 0.6$) with a tendency to adopt orthorhombic symmetry exhibit huge normal coercivity behavior at 5 K, large magnetic frustration with marginal ferromagnetism.

Let us discuss the cause of Fe/Re antisite disorder first. It is well known that the larger the difference in size of the B and B' atoms or the charges of the B and B' ions, the more chance that the compounds will have an ordered structure over the B and B' sites, the same holds for the A cations. As reported for the $(La_{1+x}M_{1-x})$-$CoRuO_6$ (M=Ca, Sr) [11], there are two potential causes for Fe/Re antisite disorder in $Ca_{2-x}La_xFeReO_6$. One cause is a reduction in size and charge difference between the average Fe and Re states. Another one is the random strain field resulting from the A-site La/Ca disorder. The structural disorder on the A-sites that can be quantified, using the statistical size variance [31]. $\delta^2 = \langle r_A^2 \rangle - \langle r_A \rangle^2$. When only one type of ion is present, then $\delta^2 = 0$. The ratio of δ^2 increases as with an La doping. The coupling between A-site size variance and B-site disorder will be maximal for x=0.8, in which the A-site size variance is largest, $\delta^2 = 3.11 \times 10^{-4}$ Å. Now, it is worth comparing these results with those in related double pervoskites $Sr_{2-x}La_xFeReO_6$ [10]. First of all, both the values of δ^2 and the degree of ASDs increase, when the increase of an La doping. However, the relation between δ^2 and ASDs is relatively weaker in $Sr_{2-x}La_xFeReO_6$ than that in $Ca_{2-x}La_xFeReO_6$. For instance, $Sr_{1.5}La_{0.5}FeReO_6$ has a 5.5% concentration of ASDs, where the A-site variance is the largest, i.e. $\delta^2 = 16.57 \times 10^{-4}$ Å. It seems that the random distribution of La^{3+} in the Ca^{2+} matrix, inherent to the synthetic process, could be the origin of the increase of ASDs, because the enhancement of ASDs is companied by the increase of δ^2. However, we must examine the starting materials. The initial Re valence has been controlled by the ratio of ReO_3/Re, i.e. +4.5 for x=0.8., while the initial Fe valence was kept at +3. Therefore, it is impossible to exclude a reduction in size and charge differences between the average Fe and Re states although secondary phase has been present. In general, two potential causes about Fe/Re antisite disorder must be taken into account in $Ca_{2-x}La_xFeReO_6$.

The second aspect is the possible relationship between the huge increase of coercivity and promotion of ASDs in the La-riched compounds. In the FeRe compounds, the increasing coercivity below Ts attributed to a large intrinsic magnetic anisotropy. The large intrinsic magnetic anisotropy takes place

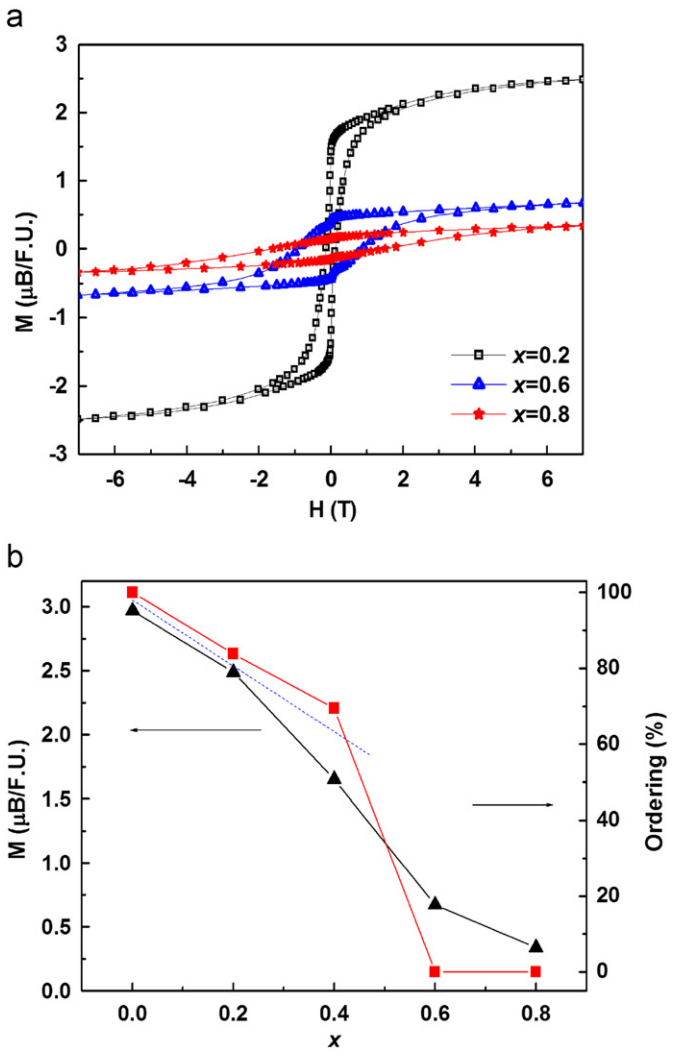

Fig. 5. (a) Field dependence of magnetization of the $Ca_{2-x}LaxFeReO_6$ samples taken at 5 K. (b) Saturation magnetization M (left axis) and degree of ordering in the B position (right axis) vs. La content (x) in $Ca_{2-x}La_xFeReO_6$ samples.

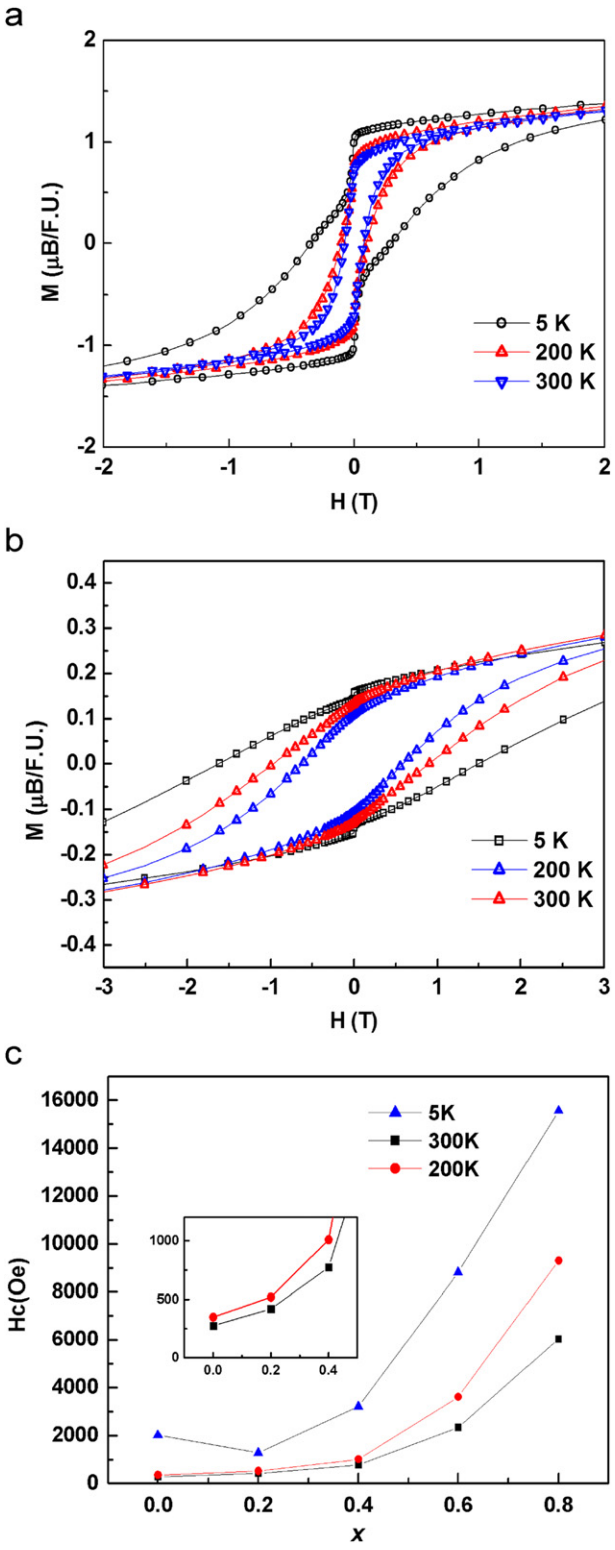

Fig. 6. Magnetization hysteresis loops at selected temperature for (a) $x=0.4$ and (b) $x=0.8$ samples. (c) Coercive field vs. La content (x) at selected temperature.

with an orbital anisotropic electron density, which couples to the lattice via crystal-field effects, and a spin-orbit interaction that couples the orbital with spin magnetic moments. Before going into the details, we must recall that at a low temperature, the undoped sample is divided into soft magnetic phase ($M1$) and hard magnetic phase ($M2$), which are competing for the ground state. $M1$ is predominant above Ts and $M2$ below Ts, but both phases coexist in a wide temperature range [5,25]. $M1$ is a collinear ferrimagnet (Re magnetic moment antiparallel to the Fe magnetic moment) with saturation magnetization of 3 μB/f.u. and the easy magnetization axis lies in the ac plane. $M2$ shows a ferrimagnetic ordering with an antiferromagnetic canting and the saturation magnetization is lower than 3 μB/f.u. The easy magnetization axis of an $M2$ is parallel to the b-axis.

In the highly doped compounds ($x \geq 0.6$), a gradual increase of coercivity with the La doping can be connected with an increase of an $M2$ phase, which is characteristic of relative high orbital moment and ASDs which promote antiferromagnetism (AFM)($M1$ phase almost vanished). It should be noted that, $M2$ phase has shorter b-axis, longer a and c axes [5]. The variation of b-axis in La-substituted compounds is in agreement with the fact that the degree of the b-axis expansion is relatively smaller, compared with a- or c-axis with the increase of an La doping. We propose that a strong magnetoelastic coupling exists in both $M2$ and AFM phases. In addition, we should take account of the relationship between smaller saturation magnetization of the highly doped samples and the concentration of ASDs. In fact, the rapid reduction of saturation magnetization relative to the decrease of the degree of ordering can support the above explanation, when the mixture

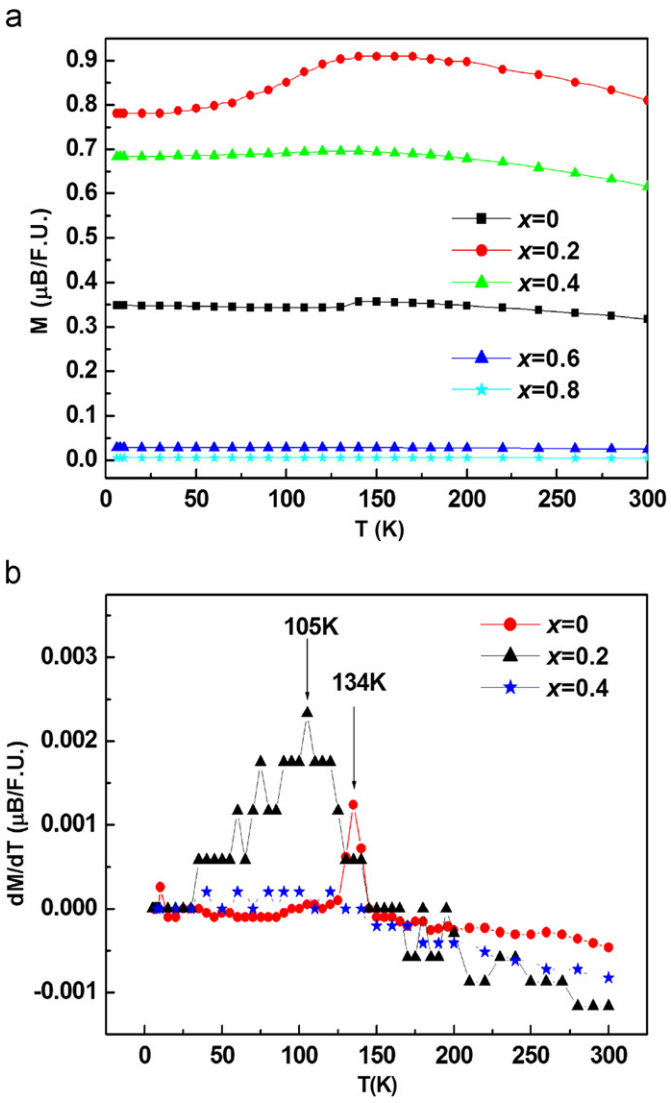

Fig. 7. (a) Magnetization vs. temperature at low-field (1000 Oe) for the $Ca_{2-x}La_x$-$FeReO_6$ samples. (b)The derivative of magnetization vs. temperature for the $Ca_{2-x}La_xFeReO_6$ samples and the maximum is marked.

of *M*2 and AFM phases became predominate in the highly doped compounds.

In low doping region ($x \leq 0.4$), the compounds exhibit abnormal magnetic behavior, which is a consequence of *M*1 and *M*2 phases, because of the low concentration of ASDs. The different phases with different magnetic properties overlap in the compounds and a simultaneous magnetic transition between these phases occurs at T_S. Moreover there is a trend to increase T_c with an increasing La doping. These complicated behaviors can be regarded as the competition of several effects stemming from the substitution of an Sr^{2+} by an La^{3+} ions. Among them, the most important ones are the steric effect and electronic band filling, which affect T_c in opposite ways. As shown in Fig. 4 and Table 3, the bond distances increase and the bond angles decrease upon an La doping. Both facts are known to reduce the hopping interaction strengths. That is, the structural contribution would reduce T_c, as has been previously proposed [8]. An additional ferromagnetic mechanism to the usual Fe(t_{2g})–Re(t_{2g}) pdd-π coupling must be invoked in order to explain the observed high T_c. Fe–O–Re angle deviation from 180° allows the Fe (e_g)–Re(e_g) pdd-δ coupling and further increase ferromagnetic interaction. This hypothesis was supported by the measurements of XANES, which revealed the

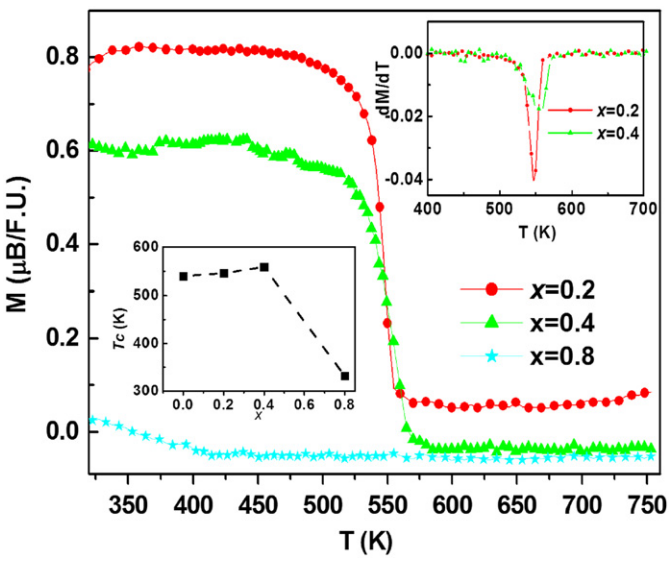

Fig. 8. Magnetization at 1000 Oe vs. temperature, for $Ca_{2-x}La_xFeReO_6$ samples. Lower inset shows the variation of the Curie temperature along the series, calculated from the first derivative of the *M*(*T*) curve (upper inset).

Lanthanide-doping does not affect the electronic state of Re cations [32].

In summary, an increase of T_c is obtained only at a low La doping region. At high La content with a high concentration of ASDs, T_c decrease rapidly. The origin of slight increasing T_c was related to Fe–O–Re angle deviation from 180°, which allows the Fe(e_g)–Re(e_g) pdd-δ coupling to further increase ferromagnetic interaction. Three different phases (*M*1, *M*2 and AFM) with different magnetic properties are competing for the ground state, which correlate with a simultaneous structural/magnetic transition.

Acknowledgments

We thank the National Natural Science Foundation of China for financial support of (Grant nos. 20771100, 20831004, 90922015 and 20921002) and CIAC, CAS (CX07QZJC30).

References

[1] K.-I. Kobayashi, T. Kimura, Y. Tomioka, H. Sawada, K. Terakura, Y. Tokura, Phys. Rev. B 59 (1999) 11159.
[2] W. Prellier, V. Smolyaninova, A. Biswas, C. Galley, R.L. Greene, K. Ramesha, J. Gopalakrishnan, J. Phys.: Condens. Matter 12 (2000)) 965.
[3] K.-I. Kobayashi, T. Kimura, H. Sawada, K. Terakura, Y. Tokura, Nature 395 (1998) 667.
[4] J. Longo, R. Ward, J. Am. Chem. Soc 83 (1961) 2816.
[5] E. Granado, Q. Huang, J.W. Lynn, J. Gopalakrishnan, R.L. Greene, K. Ramesha, Phys. Rev. B 66 (2002) 064409.
[6] J.J. Blanco, T. Hernández, L.M. Rodríguez-Martínez, M. Insausti, J.M. Barandiarán, J. Greneche, T. Rojo, J. Mater. Chem. 11 (2001) 253.
[7] H. Wu, Phys. Rev. B 64 (2001) 125126.
[8] J. Navarro, C. Frontera, L.I. Balcells, B. Martínez, J. Fontcuberta, Phys. Rev. B 64 (2001) 092411.
[9] D. Sánchez, J.A. Alonso, M. García-Hernández, M.J. Martínez-Lope, J.L. Martínez, A. Mellergard, Phys. Rev. B 65 (2002) 104426.
[10] J. Blasco, J.A. Rodríguez-Velamazán, C. Ritter, J. Seséc, J. Stankiewicz, J. Herrero-Martín, Solid State Sci. 11 (2009) 1535.
[11] Jan-Willem G. Bos, J.P. Attfield, Phys. Rev. B 69 (2004) 094434.
[12] R.D. Shannon, Acta Crystallogr. A 32 (1976) 751.
[13] (a) A. Boultif, D. Louer, J. Appl. Crystallogr. 37 (2004) 724;
(b) D. Louer, M. Louer, J. Appl. Crystallogr. 5 (1972) 271;
(c) A. Boultif, D. Louer, J. Appl. Crystallogr. 24 (1991) 987.
[14] P.-E. Werner, L. Eriksson, M. Westdahl, J. Appl. Crystallogr. 18 (1985) 367.
[15] J.W. Visser, J. Appl. Crystallogr. 2 (1969) 89.
[16] R.W. Cheary, A.A. Coelho, in: Programs XFIT and FOURYA, Daresbury Laboratory, Warrington, 1996.
[17] J.W. Visser, Powder Diffr. 1 (1986) 66.

[18] A. LeBail, H. Duroy, J.L. Fourquet, Mater. Res. Bull. 23 (1988) 447.
[19] A.C. Larson, R.B. Von Dreele, in: General Structure Analysis System (GSAS), Los Alamos National Laboratory, 2000;
B.H. Toby, J. Appl. Crystallogr. 34 (2001) 210.
[20] G.M. Sheldrick, in: SHELXL-97, A Program for Crystal Structure Refinement, University of Geottingen, Germany, 1997.
[21] P.T. Beurskens, G. Admiraal, G. Beurskens, W.P. Bosman, R. de Gelder, R. Israel, J.M. Smits, in: dirdif-99: The dirdif-99 Program System, Nijmegen, The Netherlands, 1999.
[22] A. Le Bail, OVERLAP: a program to obtain a reduced dataset by elimination of the reflections overlapping too much, Version D. Le Mans Cedex, France, 1999.
[23] L.J. Farrugia, in: WINGX, A Windows Program for Crystal Structure Analysis, University of Glasgow, UK, 1988.
[24] V. Ting, Y. Liu, R.L. Withers, L. Norén, M. James, J.D. Fitz Gerald, J. Solid State Chem. 179 (2006) 551.
[25] W. Westerburg, O. Lang, C. Ritter, C. Felser, W. Tremel, G. Jakob, Solid State Commun. 122 (2002) 201.
[26] P.M. Woodward, Acta Crystallogr. B 53 (1997) 32.
[27] A.M. Glazer, Acta Crystallogr. B 28 (1972) 3384.
[28] M. Gateshki, J.M. Igartua, Mater. Res. Bull. 38 (2003) 1893.
[29] J.M. DeTeresa, D. Serrate, J. Blasco, M.R. Ibarra, L. Morellon, Phys. Rev. B 69 (2004) 144401.
[30] M. Medarde, J. Mesot, P. Lacorre, S. Rosenkranz, P. Fischer, K. Gobrecht, Phys. Rev. B 52 (1995) 9248.
[31] J.P. Attfield, Chem. Mater. 10 (1998) 3239.
[32] J. Blasco, J.M. Michalik, J. García, G. Subías, J.M. DeTeresa, Phys. Rev. B 76 (2007) 144402.